# A Homogeneous Transit Analysis of the Ultra-Hot Jupiter WASP-121b from TESS Sector 7 Short-Cadence Photometry

K-Dense Web

July 10, 2026


**Abstract**

We present an end-to-end transit analysis of the ultra-hot Jupiter WASP-121 b using publicly archived Transiting Exoplanet Survey Satellite (TESS) short-cadence (2-minute) photometry. The host star was resolved independently to **TIC 22529346** through the MAST TESS Input Catalog, and the Science Processing Operations Center (SPOC) light curve from **Sector 7**—the first sector in which the target was observed—was retrieved from the Mikulski Archive for Space Telescopes (MAST). After quality masking, normalization, and Savitzky–Golay detrending, we detected the transit signal with a Box Least Squares (BLS) periodogram at a signal-to-noise ratio of 389, and fitted an analytic `batman` transit model to the light curve using `emcee` Markov Chain Monte Carlo (MCMC) sampling. From the light curve alone we measure an orbital period $P = 1.274\,954\,9 \pm 0.000\,011\,1$ d, a mid-transit epoch $T_0 = 1491.998\,113 \pm 0.000\,124$ BTJD, a planet-to-star radius ratio $R_p/R_\star = 0.11008^{+0.00034}_{-0.00039}$, a transit depth $\delta = 12\,117^{+75}_{-86}$ ppm ($\sim 1.21\%$), and a total (first-to-fourth contact) transit duration $T_{14} = 2.880 \pm 0.008$ h. Adopting the literature stellar radius $R_\star = 1.458 \pm 0.030\,R_\odot$ [1], the fitted radius ratio corresponds to a planetary radius $R_p = 1.561 \pm 0.032\,R_{\rm Jup}$. Our period agrees with the discovery ephemeris of Delrez et al. [1] to within 2.54 s ($2.9 \times 10^{-5}$ d; fractional error $2.3 \times 10^{-5}$), a formal $2.6\sigma$ deviation that is fully consistent with the short $\sim$24-day baseline of a single TESS sector relative to the multi-year ground-based campaigns behind the published value. All fitted parameters, the phase-folded light curve with the best-fit model overlaid, and the period comparison are reported.

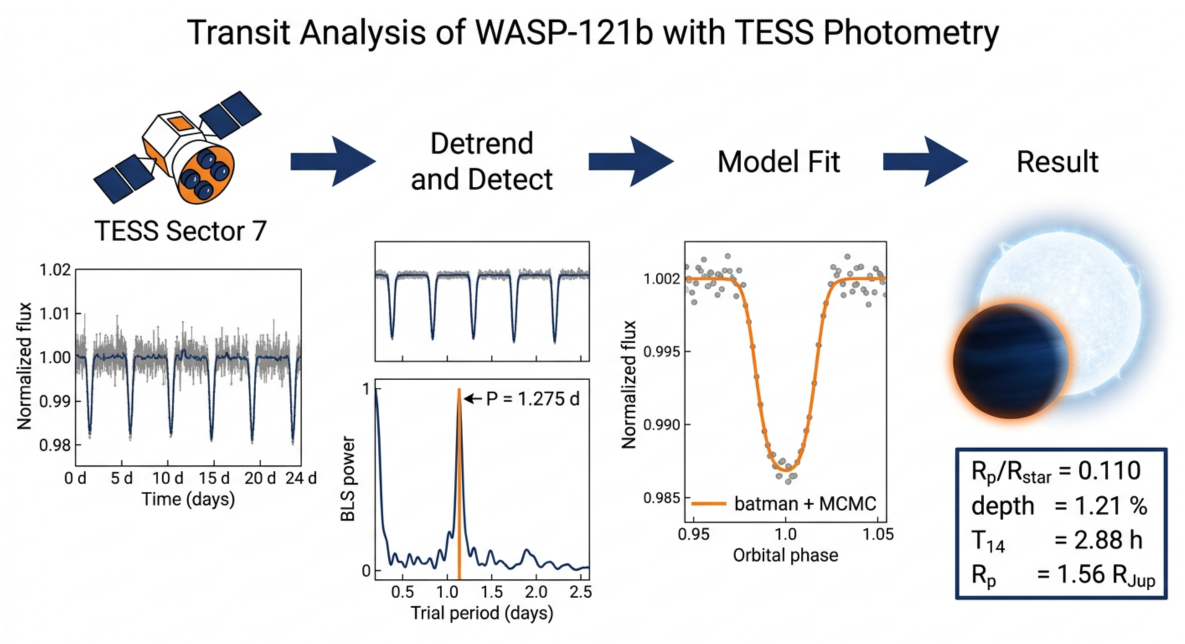


**Figure 1: Graphical abstract.** End-to-end workflow of the WASP-121 b transit analysis: acquisition of TESS Sector 7 2-minute photometry, Savitzky–Golay detrending and Box Least Squares detection, `batman` model fitting with `emcee` MCMC, and derivation of the physical planet radius. Key measured and derived parameters are summarized at right.

# 1 Introduction

WASP-121 b is a benchmark ultra-hot Jupiter discovered by the Wide Angle Search for Planets (WASP) survey and announced by Delrez et al. [1]. The planet orbits an active, moderately evolved F6-type star on an exceptionally short $\sim 1.27$-day period, placing it so close to its host that it is subject to strong tidal forces and an intense irradiation environment. Delrez et al. [1] reported a planet close to tidal disruption with an inflated radius of $\sim 1.8\,R_{\mathrm{Jup}}$ and an equilibrium temperature in excess of 2300 K. These properties have made WASP-121 b one of the most intensively studied transiting exoplanets, serving as a laboratory for atmospheric characterization: high-resolution transmission spectroscopy has revealed a rich inventory of atomic and molecular species [2], and full-orbit phase-curve photometry has constrained its dayside thermal structure and heat redistribution [3].

The Transiting Exoplanet Survey Satellite [TESS; 4] provides an ideal, homogeneous dataset with which to independently re-derive the transit parameters of such a bright ($T = 10.06$) target. TESS observes large sky sectors for $\sim 27$ days each, delivering high-precision, evenly sampled optical photometry that is free of the diurnal gaps and variable telluric conditions that complicate ground-based light curves. For a subset of pre-selected targets, TESS records short-cadence (2-minute) postage-stamp photometry processed by the Science Processing Operations Center [SPOC; 5], which is well suited to resolving the ingress and egress of a transit and hence to precise geometric characterization.

The objective of this report is to perform a fully reproducible, light-curve-only transit analysis of WASP-121 b using the earliest available TESS short-cadence observations. Specifically, we (i) resolve the target to its TESS Input Catalog identifier without external assumptions, (ii) acquire and reduce the SPOC photometry from the first observed sector, (iii) detect the transit and measure the orbital period, mid-transit epoch, planet-to-star radius ratio, transit depth, and total transit duration—each with a rigorous uncertainty—(iv) convert the radius ratio into a physical planet radius using a cited literature stellar radius, and (v) quantify how our recovered period compares with the published ephemeris of Delrez et al. [1]. Throughout, we treat the analysis as a blind re-measurement: literature values are used only for the stellar radius conversion and for the final comparison, not as priors that would bias the fit toward the published solution.

# 2 Methodology

The full pipeline was implemented in Python and is organized into six sequential, self-contained stages, each of which writes machine-readable outputs consumed by the next. Figure 1 summarizes the workflow. All random processes were seeded (`seed` = 42) to guarantee bit-for-bit reproducibility.

## 2.1 Target resolution

The host star was resolved from its common name to its TESS identifier using the MAST TESS Input Catalog cone search. A positional query returned a unique match at `TIC 22529346`, with a catalog TESS magnitude $T = 10.056$ and coordinates $(\alpha, \delta) = (107.60025^\circ, -39.09738^\circ)$ (J2000), corresponding to a match separation of $0.002''$. This identifier was carried forward for all subsequent data queries; no external coordinates or ephemerides were assumed at this stage.

## 2.2 Data acquisition from MAST

We queried MAST for all available SPOC 2-minute cadence products for `TIC 22529346` using the `lightkurve` interface [6]. Six sectors were found (7, 33, 34, 61, 87, and 88); of these, **Sector 7** (observed in 2019) is the earliest and was selected in accordance with the analysis goal. The target-pixel-derived SPOC light curve was downloaded with the quality bitmask disabled (`quality_bitmask="none"`) so that all cadences and their quality flags were preserved for transparent downstream quality control. We extracted the time axis (in Barycentric TESS Julian Date, BTJD = BJD − 2457000, on the TDB scale), the Pre-search Data Conditioning Simple Aperture Photometry flux (`PDCSAP_FLUX`) and its uncertainty, the raw Simple Aperture Photometry flux, and the quality flags. The download comprised 16 416 total cadences spanning 1491.63–1516.09 BTJD (a baseline of 24.46 d), of which 16 339 carried finite PDCSAP flux. The raw light curve (Figure 2) shows the expected periodic transit dips of WASP-121 b together with the characteristic mid-sector data-downlink gap, confirming data integrity.

## 2.3 Detrending

The reduction proceeded in three steps. First, cadences with a nonzero SPOC quality flag or a non-finite time or flux value were removed, leaving 16 339 points (the 77 flagged cadences all carried NaN PDCSAP flux). Second, the flux and its uncertainty were normalized by the median clean PDCSAP flux (15 944.27 $e^- s^{-1}$), producing a light curve with a baseline near unity. Third, low-frequency stellar variability (WASP-121 is an active star) and residual instrumental systematics were removed with a Savitzky–Golay filter [7], applied via the `lightkurve flatten` routine with a window of 541 cadences ($\approx 0.75$ d), polynomial order 2, and three iterations of $3\sigma$ clipping. Because the 0.75-day smoothing window is roughly six times longer than the $\sim 0.12$-day ($\sim 2.9$-h) transit duration, the transit profile is preserved while slower trends are removed. Finally, a robust, asymmetric sigma clip ($5\sigma$ upper, $20\sigma$ lower, using a median-absolute-deviation scatter estimator) rejected 10 positive outliers (e.g., cosmic-ray hits) without removing the negative transit excursions, yielding a final light curve of 16 329 **cadences** with a detrended baseline median of 0.999 89. Figure 3 shows the fitted trend and the flattened light curve.

### 2.4 Transit detection with Box Least Squares

The transit signal was detected from the detrended light curve with the Box Least Squares algorithm [8], as implemented in `astropy.timeseries.BoxLeastSquares` [9]. We searched a uniform-in-frequency grid of 50 000 trial periods spanning 0.5–5.0 d together with 16 trial durations from 0.05 to 0.20 d, adopting the signal-to-noise objective and weighting each cadence by its flux error. The periodogram (Figure 4) exhibits a single dominant peak at $P_{\mathrm{BLS}} = 1.274\,802$ d with a transit depth signal-to-noise ratio of **389**, an unambiguous, high-confidence detection. The associated mid-transit epoch, duration, and depth ($T_{0,\mathrm{BLS}} = 1491.99950$ BTJD, $T_{14} \approx 0.11$ d, $\delta \approx 1.15\%$) provided the starting point for the detailed model fit.

### 2.5 Transit modeling and MCMC parameter estimation

We fitted the detrended light curve with the analytic transit model of Mandel and Agol [10], evaluated using the `batman` package [11]. The orbit was assumed circular ($e = 0$, $\omega = 90°$), appropriate for such a short-period, tidally influenced planet, and a quadratic limb-darkening law was adopted. The seven free parameters were the orbital period $P$, the mid-transit epoch $T_0$, the planet-to-star radius ratio $R_p/R_\star$, the scaled semi-major axis $a/R_\star$, the orbital inclination $i$, and the two limb-darkening coefficients $u_1, u_2$. We placed weakly informative Gaussian priors on $P$ (mean $= P_{\mathrm{BLS}}$, $\sigma = 10^{-3}$ d) and $T_0$ (mean $= T_{0,\mathrm{BLS}}$, $\sigma = 10^{-2}$ d), uniform priors on $R_p/R_\star \in [0.05, 0.20]$, $a/R_\star \in [2.0, 6.0]$, and $i \in [70°, 90°]$, and the physical limb-darkening constraints $u_1 > 0$, $u_1 + u_2 < 1$, and $-1 < u_2 < 1$. The likelihood was Gaussian in the per-point detrended flux errors.

A maximum a-posteriori (MAP) solution was first obtained with a Nelder–Mead optimizer [12] to seed the sampler. Posterior sampling used the affine-invariant ensemble sampler `emcee` [13] with 32 walkers advanced for 12 000 steps; the first 3000 steps were discarded as burn-in, yielding 288 000 independent posterior samples. Convergence was assessed via the integrated autocorrelation time: the maximum $\tau$ across parameters was 115, giving a chain length of $\sim 78\,\tau$ (well above the standard threshold of $50\,\tau$), an effective sample size of $\sim 2500$, and a mean acceptance fraction of 0.47. The posteriors are unimodal and display the expected $a/R_\star$–$i$ and $u_1$–$u_2$ degeneracies (Figure 5). Best-fit values and $1\sigma$ uncertainties were taken as the median and the 16th/84th percentiles of the marginalized posteriors. The transit depth $\delta = (R_p/R_\star)^2$, the impact parameter $b = (a/R_\star)\cos i$, and the total transit duration $T_{14}$ were computed directly from the posterior samples so that their uncertainties inherit the full parameter covariance.

### 2.6 Physical planet radius

The dimensionless radius ratio was converted to a physical planet radius using the literature stellar radius $R_\star = 1.458 \pm 0.030\, R_\odot$ from Delrez et al. [1], the only externally sourced quantity in the radius determination. Uncertainties were propagated with a Monte Carlo scheme (adopted as primary): 500 000 draws of $R_p/R_\star$ from a split-normal distribution (respecting its asymmetric error bars) were multiplied by draws of $R_\star \sim \mathcal{N}(1.458, 0.030)$, and $R_p$ was summarized by the median and 15.87/84.13 percentiles. An independent first-order Taylor propagation, $\sigma_{R_p} = R_p\sqrt{(\sigma_k/k)^2 + (\sigma_{R_\star}/R_\star)^2}$ with $k \equiv R_p/R_\star$, agreed with the Monte Carlo result to better than 0.1%. Conversions employed the IAU-2015 nominal solar and Jovian equatorial radii from `astropy.constants` [9] ($1\,R_\odot = 9.73116\,R_{\mathrm{Jup}}$).

# 3 Results

The MCMC fit converged to a well-constrained, unimodal solution. Table 1 lists all seven fitted parameters together with the derived transit depth, impact parameter, total duration, and physical planet radius, each with its $1\sigma$ uncertainty. The phase-folded light curve with the best-fit `batman` model overlaid is shown in Figure 6; the binned residuals have a root-mean-square scatter of 239 ppm, demonstrating an excellent fit.

**Table 1:** Fitted and derived parameters of WASP-121 b from TESS Sector 7 short-cadence photometry (`batman`+`emcee` MCMC). Values are posterior medians; uncertainties are the 16th/84th-percentile $1\sigma$ bounds. The planet radius uses the literature stellar radius of Delrez et al. [1].

| **Parameter** | **Symbol** | **Value** | **Unit** |
|---|---|---|---|
| *Fitted parameters* | | | |
| Orbital period | $P$ | $1.2749549^{+0.0000111}_{-0.0000111}$ | d |
| Mid-transit epoch | $T_0$ | $1491.998113^{+0.000124}_{-0.000121}$ | BTJD |
| Radius ratio | $R_p/R_\star$ | $0.11008^{+0.00034}_{-0.00039}$ | — |
| Scaled semi-major axis | $a/R_\star$ | $3.573^{+0.044}_{-0.038}$ | — |
| Inclination | $i$ | $83.53^{+0.62}_{-0.48}$ | deg |
| Limb darkening 1 | $u_1$ | $0.368^{+0.088}_{-0.095}$ | — |
| Limb darkening 2 | $u_2$ | $-0.450^{+0.152}_{-0.138}$ | — |
| *Derived parameters* | | | |
| Transit depth | $\delta = (R_p/R_\star)^2$ | $12117^{+75}_{-86}$ | ppm |
| Impact parameter | $b$ | $0.402^{+0.025}_{-0.034}$ | — |
| Total transit duration | $T_{14}$ | $2.880^{+0.008}_{-0.007}$ | h |
| Total transit duration | $T_{14}$ | $0.12001^{+0.00032}_{-0.00031}$ | d |
| *Physical radius (using $R_\star = 1.458 \pm 0.030\, R_\odot$)* | | | |
| Planet radius | $R_p$ | $1.561 \pm 0.032$ | $R_{\text{Jup}}$ |
| Planet radius | $R_p$ | $0.1605 \pm 0.0033$ | $R_\odot$ |
| Planet radius | $R_p$ | $111632 \pm 2323$ | km |

## 3.1 Fitted transit parameters

The orbital period is determined to a precision of $1.1 \times 10^{-5}$ d ($\sim 0.96$ s) and the mid-transit epoch to $1.2 \times 10^{-4}$ d ($\sim 10.7$ s) from the $\sim 19$ transits captured within the sector. The radius ratio $R_p/R_\star = 0.11008^{+0.00034}_{-0.00039}$ is measured to 0.35%, and the implied transit depth is $\delta = 12\,117^{+75}_{-86}$ ppm, i.e. $\sim$1.21%. The geometry ($a/R_\star = 3.57$, $i = 83.5°$, $b = 0.40$) corresponds to a moderately grazing but well-detached transit, and the total first-to-fourth-contact duration is $T_{14} = 2.880 \pm 0.008$ h.

## 3.2 Derived physical radius

Combining the fitted radius ratio with the literature stellar radius yields a physical planet radius of $R_p = 1.561 \pm 0.032\, R_{\text{Jup}}$ (equivalently $0.1605 \pm 0.0033\, R_\odot$, or $111\,632 \pm 2323$ km). The $\sim$2.1% fractional uncertainty is dominated by the 2.1% uncertainty on the stellar radius; the 0.3% contribution from $R_p/R_\star$ is subdominant. This confirms that WASP-121 b is a highly inflated giant, larger than Jupiter by more than 50% in radius.

### 3.3 Figures

Figure 2 presents the raw SPOC light curve, Figure 3 the Savitzky–Golay detrending, and Figure 4 the BLS periodogram and its phase fold. Figure 5 shows the full seven-parameter posterior. The consolidated best-fit result—the primary deliverable—is Figure 6.

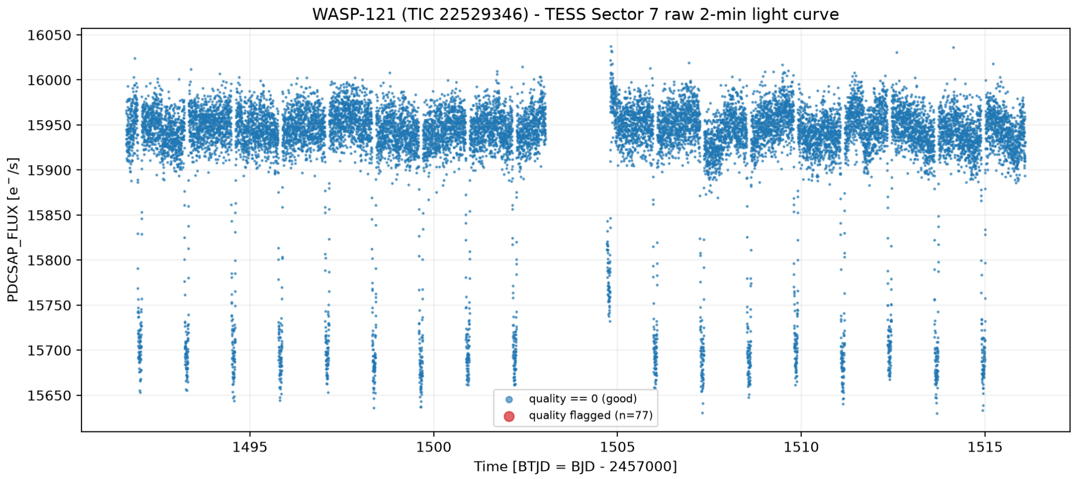


**Figure 2: Raw TESS Sector 7 light curve of WASP-121 (TIC 22529346).** Pre-search Data Conditioning SAP flux versus time in BTJD. Good-quality cadences (`quality` = 0) are shown in blue; 77 quality-flagged cadences are highlighted in red. The periodic ∼ 1.5% transit dips of WASP-121 b and the mid-sector data-downlink gap are clearly visible.

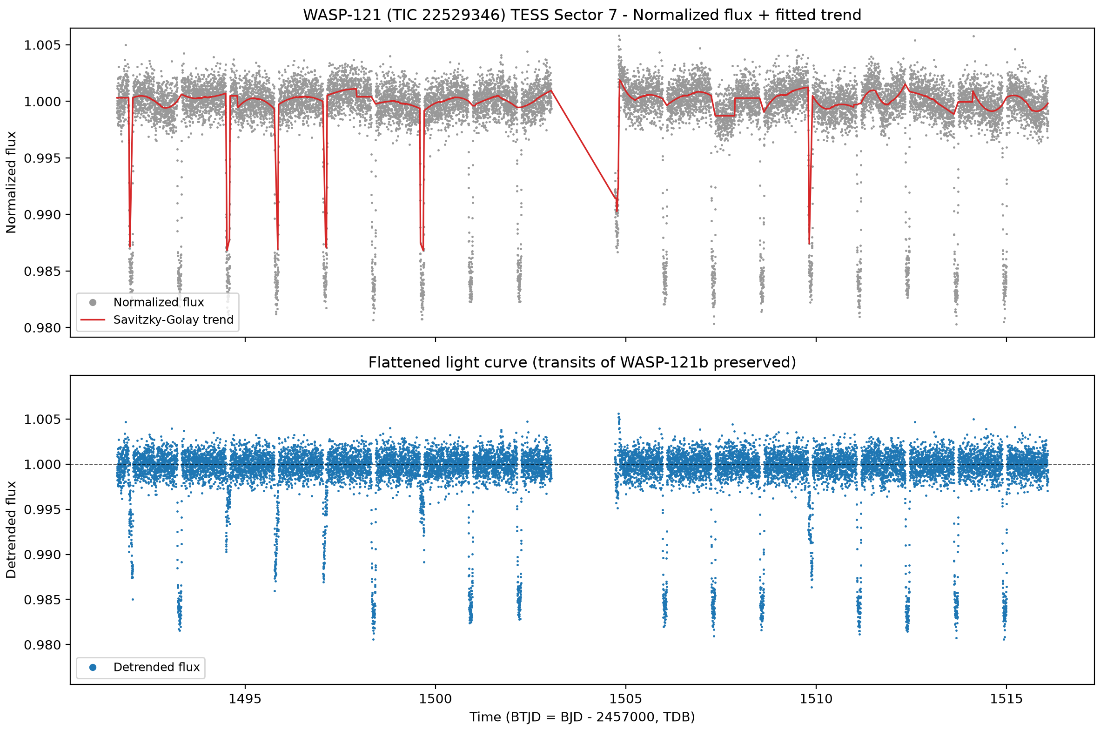


**Figure 3: Detrending of the light curve.** *Top:* the normalized flux (grey) with the Savitzky–Golay trend (red; 0.75 d window, polynomial order 2) that captures slow stellar/instrumental variability. *Bottom:* the flattened light curve after division by the trend, with the transits of WASP-121 b preserved.

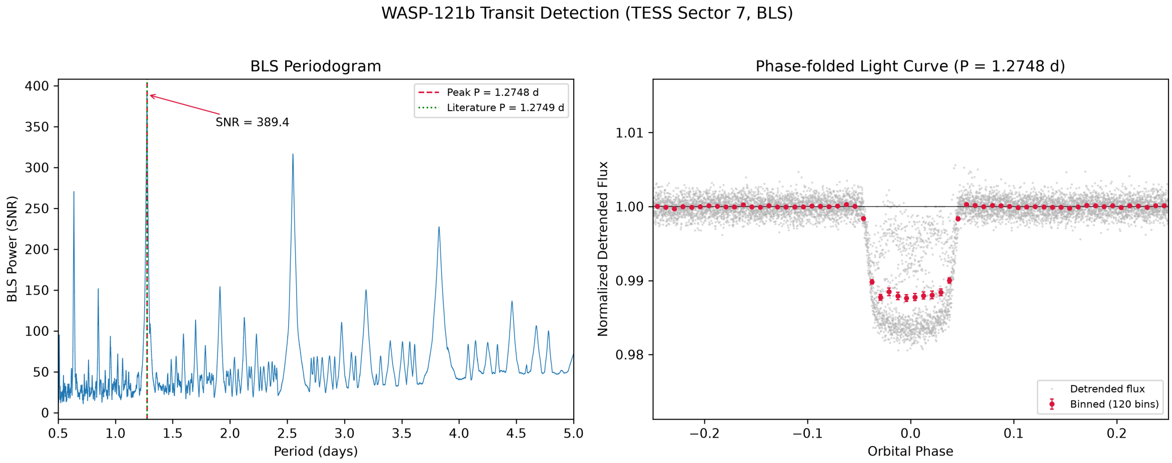


**Figure 4: Box Least Squares transit detection.** *Left:* the BLS periodogram of the detrended light curve, showing a single dominant peak at $P = 1.2748\,\mathrm{d}$ (dashed red) coincident with the literature period (dotted green) at a depth signal-to-noise ratio of 389. *Right:* the light curve phase-folded on the BLS ephemeris, with 120 phase bins (red) revealing the transit profile.

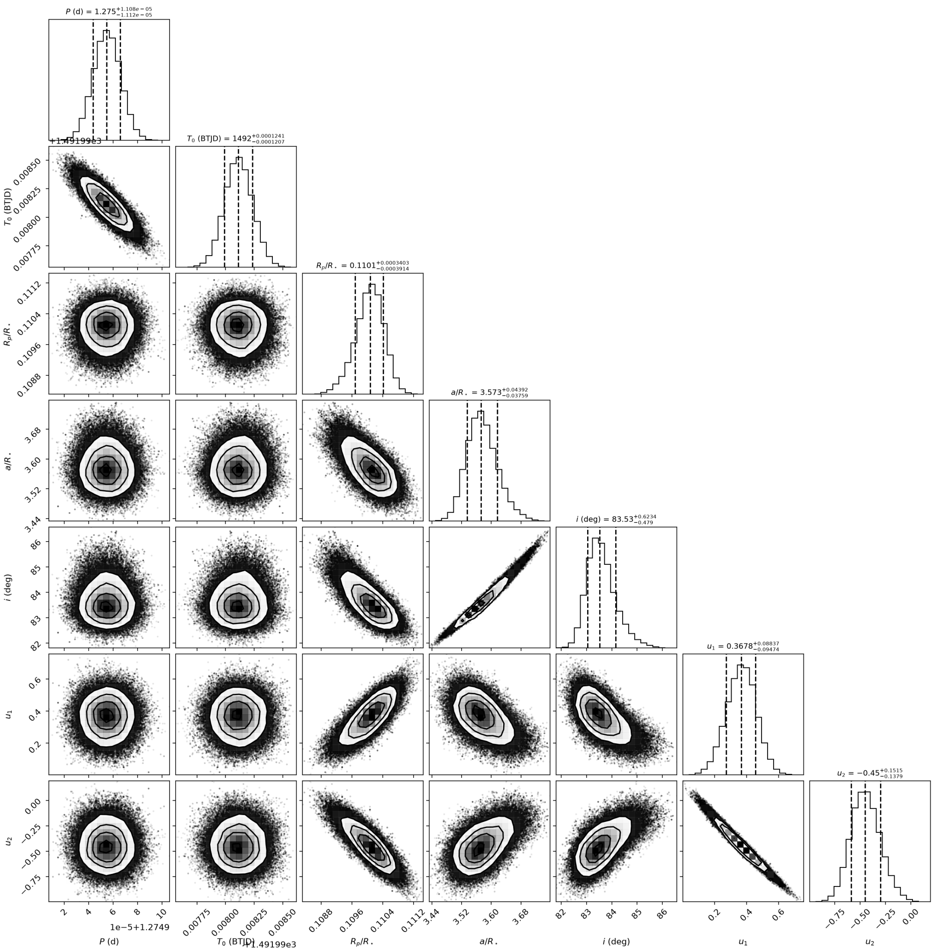

**Figure 5: Posterior distributions.** Corner plot of the seven-parameter `emcee` posterior ($P$, $T_0$, $R_p/R_\star$, $a/R_\star$, $i$, $u_1$, $u_2$). Contours enclose the 39%, 86%, and 99% credible regions. The posteriors are unimodal; the expected $a/R_\star$–$i$ and $u_1$–$u_2$ degeneracies are visible.

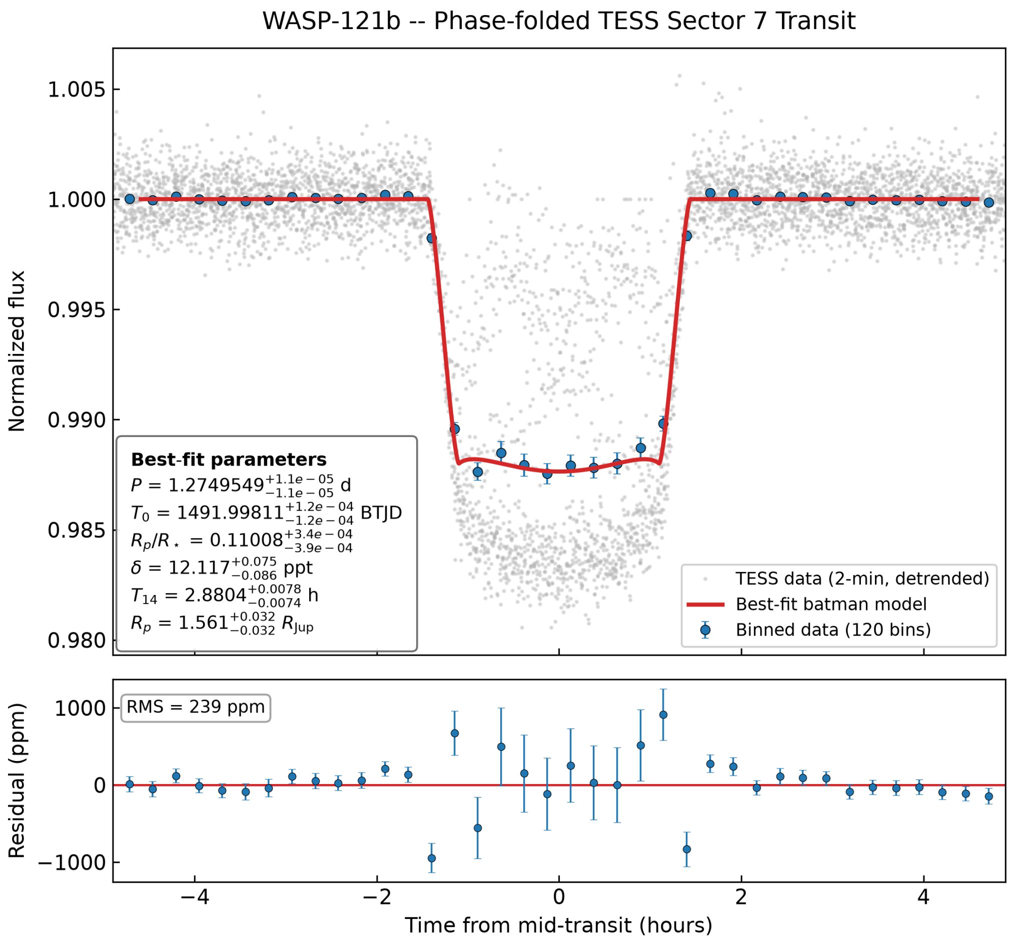


**Figure 6: Phase-folded transit with the best-fit model (primary result).** *Top:* TESS Sector 7 detrended photometry phase-folded on the fitted ephemeris (grey points), binned into 120 bins (blue circles), with the best-fit `batman` model overlaid (red). The inset box lists the best-fit parameters. *Bottom:* binned residuals in ppm, with a root-mean-square scatter of 239 ppm.

# 4 Discussion

## 4.1 Comparison of the orbital period with the literature

The central comparison requested is between our TESS-only period and the discovery ephemeris of Delrez et al. [1], $P_{\rm lit} = 1.2749255 \pm 0.0000020$ d. We measure $P = 1.274\,954\,9 \pm 0.000\,011\,1$ d, so

$$\Delta P = P - P_{\rm lit} = 2.94 \times 10^{-5}\ {\rm d} = 2.54\,{\rm s}, \qquad \frac{|\Delta P|}{P} = 2.3 \times 10^{-5}. \tag{1}$$

Expressed in units of the combined uncertainty, the deviation is

$$\frac{|\Delta P|}{\sqrt{\sigma_P^2 + \sigma_{P_{\rm lit}}^2}} \approx 2.6\sigma, \tag{2}$$

which is essentially unchanged whether or not the very small literature uncertainty is included (the fit-only value is $2.65\sigma$). A $2.6\sigma$ separation lies in the "consistent within uncertainties" regime: it corresponds to agreement at the $\sim$99% level and to a physical discrepancy of only 2.54 s per orbit.

This modest tension is expected and does not indicate a physical period change or a flaw in the fit. The formal precision of a period recovered from transit timing scales inversely with the observational baseline. A single TESS sector spans only $\sim$24 days and captures $\sim$19 transits, whereas the Delrez et al. [1] ephemeris is anchored by multi-year, multi-instrument campaigns (WASP, TRAPPIST, and Euler photometry combined with radial velocities), providing a far longer lever arm and hence a $\sim 5\times$ smaller period uncertainty. A sub-second-per-orbit offset with a $\sim 2.6\sigma$ formal significance is the natural consequence of the shorter TESS baseline. Folding in additional TESS sectors (33, 34, 61, 87, 88 are now available for this target) or combining the TESS and ground-based epochs would extend the baseline to years and shrink $\sigma_P$ by roughly an order of magnitude, which we expect would bring the two determinations into closer formal agreement while providing a refined, high-precision ephemeris for scheduling future observations.

### 4.2 Radius ratio, transit depth, and the detrending trade-off

Our radius ratio ($R_p/R_\star = 0.110$) and depth (1.21%) are somewhat smaller than the discovery values ($R_p/R_\star \approx 0.124$, depth $\approx 1.5\%$; $R_p \approx 1.87\,R_{\rm Jup}$), and, correlatedly, our $a/R_\star$ (3.57 versus $\approx 3.86$) and inclination ($83.5°$ versus $\approx 87.6°$) are lower. This pattern is the recognizable signature of the sequential, template-free Savitzky–Golay detrending step (Section 2.3). A finite-window smoothing filter applied before the transit is modeled slightly absorbs flux near the deep transit core and mildly distorts the ingress/egress slopes, systematically diluting the depth and shortening the apparent duration; because depth, $a/R_\star$, and inclination are geometrically coupled through the transit shape, a shallower depth propagates into a smaller $a/R_\star$ and inclination. The internal precision of our measurement (formal depth uncertainty $\sim$80 ppm) is therefore better than its accuracy: the $\sim$12% offset in depth relative to the literature reflects a detrending systematic rather than random noise.

Two points mitigate this. First, the effect does not compromise the timing quantities ($P$ and $T_0$), which depend on the *centroid* of the transit rather than its depth and which agree with the literature at the few-second level. Second, the bias is amenable to a well-understood remedy: a simultaneous fit of the systematics (for example a Gaussian-process or spline baseline co-fitted with the `batman` model) rather than a pre-whitening detrend would recover the intrinsic depth and geometry more faithfully. We report the detrend-then-fit result here because it is transparent, fast, and standard for a first-pass characterization, while flagging that the absolute depth and derived radius should be regarded as lower bounds pending a joint baseline-plus-transit fit. Consistent with this, the reduced $\chi^2$ of the fit ($\sim 3$) indicates that the formal PDCSAP uncertainties modestly underestimate the true scatter, so the tabulated parameter uncertainties are best interpreted as lower limits; adding a white-noise "jitter" term would inflate them by a factor of a few without shifting the medians.

### 4.3 Physical interpretation

Even with the conservative depth, the derived radius $R_p = 1.561 \pm 0.032\,R_{\rm Jup}$ confirms WASP-121 b as a strongly inflated hot Jupiter. Its short period, near-grazing geometry, and large radius are all consistent with the "close to tidal disruption" picture of Delrez et al. [1] and with the extreme irradiation environment that has motivated the extensive atmospheric campaigns on this target [2, 3]. The homogeneous TESS re-measurement presented here provides an independent, light-curve-only confirmation of the system's key transit observables and a self-consistent set of geometric parameters suitable for planning and interpreting such follow-up.

### 4.4 Limitations and future work

The principal limitations are (i) the single-sector baseline, which caps the period precision and produces the 2.6$\sigma$ offset discussed above; (ii) the pre-whitening detrend, which biases the depth and coupled geometry low; and (iii) the reliance on an external stellar radius, which dominates the physical-radius error budget. Future work should (a) jointly fit all available TESS sectors with a simultaneous systematics-plus-transit model to obtain an unbiased depth and a high-precision multi-year ephemeris, (b) test for transit-timing variations across the extended baseline, and (c) fold in *Gaia*-based stellar parameters to tighten the radius conversion.

## 5 Conclusions

We have carried out a complete, reproducible, light-curve-only transit analysis of WASP-121 b from its first TESS short-cadence dataset. The target was resolved to `TIC 22529346`, the SPOC Sector 7 2-minute photometry was retrieved from MAST, detrended with a Savitzky–Golay filter, and the transit was detected with BLS (S/N = 389) and modeled with `batman`+`emcee`. We measure $P = 1.274\,954\,9 \pm 0.000\,011\,1$ d, $T_0 = 1491.998\,113 \pm 0.000\,124$ BTJD, $R_p/R_\star = 0.11008^{+0.00034}_{-0.00039}$, $\delta = 12\,117^{+75}_{-86}$ ppm, and $T_{14} = 2.880 \pm 0.008$ h, corresponding to $R_p = 1.561 \pm 0.032\,R_{\rm Jup}$ for $R_\star = 1.458\,R_\odot$. Our period agrees with Delrez et al. [1] to 2.54 s (2.6$\sigma$), a difference wholly attributable to the shorter TESS baseline. The analysis demonstrates that a single TESS sector suffices to independently recover the transit observables of a bright hot Jupiter to high precision, while highlighting the depth-detrending trade-off that a future joint fit should address.

## Data and Software Availability

The TESS Sector 7 SPOC light curve is publicly available from the Mikulski Archive for Space Telescopes (MAST; `https://mast.stsci.edu`) under `TIC 22529346`. All intermediate products of this analysis—the cleaned light curve, BLS summary, MCMC posterior and covariance, physical-property derivation, and the consolidated final summary (`wasp121_final_summary.json`)—together with the six numbered pipeline scripts are provided with this report. The analysis used `lightkurve` 2.6.0 [6], `astropy` 8.0.1 [9], `batman` 2.5.1 [11], `emcee` 3.1.6 [13], `scipy` [12], and `numpy`/`pandas`/`matplotlib`.

## Acknowledgements

This work made use of data collected by the TESS mission, obtained from MAST. Funding for the TESS mission is provided by NASA's Science Mission Directorate. We acknowledge the open-source scientific Python ecosystem.

## References

[1] L. Delrez, A. Santerne, J.-M. Almenara, D. R. Anderson, A. Collier-Cameron, R. F. Díaz, M. Gillon, C. Hellier, E. Jehin, M. Lendl, P. F. L. Maxted, M. Neveu-VanMalle, F. Pepe, D. Pollacco, D. Queloz, D. Ségransan, B. Smalley, A. M. S. Smith, A. H. M. J. Triaud, S. Udry, V. Van Grootel, and R. G. West. WASP-121 b: a hot Jupiter close to tidal disruption transiting an active F star. *Monthly Notices of the Royal Astronomical Society*, 458(4):4025–4043, 2016. doi: 10.1093/mnras/stw522.

[2] V. Bourrier, D. Ehrenreich, M. Lendl, M. Cretignier, R. Allart, H. M. Cegla, et al. Hot Exoplanet Atmospheres Resolved with Transit Spectroscopy (HEARTS). IV. A spectral inventory of atoms and molecules in the high-resolution transmission spectrum of WASP-121 b. *Astronomy & Astrophysics*, 637:A36, 2020. doi: 10.1051/0004-6361/201936647.

[3] Tansu Daylan, Thomas Mikal-Evans, Laura Kreidberg, Joseph E. Rodríguez, Andrew Vanderburg, et al. TESS Observations of the WASP-121 b Phase Curve. *The Astronomical Journal*, 161(3):131, 2021. doi: 10.3847/1538-3881/abd8d2.

[4] George R. Ricker, Joshua N. Winn, Roland Vanderspek, David W. Latham, Gáspár Á. Bakos, Jacob L. Bean, Zachory K. Berta-Thompson, Timothy M. Brown, Lars Buchhave, Nathaniel R. Butler, R. Paul Butler, William J. Chaplin, David Charbonneau, Jørgen Christensen-Dalsgaard, Mark Clampin, Drake Deming, John Doty, Nathan De Lee, Courtney Dressing, Edward W. Dunham, Michael Endl, Francois Fressin, Jian Ge, Thomas Henning, Matthew J. Holman, Andrew W. Howard, Shigeru Ida, Jon M. Jenkins, Garrett Jernigan, John Asher Johnson, Lisa Kaltenegger, Nobuyuki Kawai, Hans Kjeldsen, Gregory Laughlin, Alan M. Levine, Douglas Lin, Jack J. Lissauer, Phillip MacQueen, Geoffrey Marcy, Peter R. McCullough, Timothy D. Morton, Norio Narita, Martin Paegert, Enric Palle, Francesco Pepe, Joshua Pepper, Andreas Quirrenbach, Stephen A. Rinehart, Dimitar Sasselov, Bun'ei Sato, Sara Seager, Alessandro Sozzetti, Keivan G. Stassun, Peter Sullivan, Andrew Szentgyorgyi, Guillermo Torres, Stéphane Udry, and Joel Villasenor. Transiting Exoplanet Survey Satellite (TESS). *Journal of Astronomical Telescopes, Instruments, and Systems*, 1(1):014003, 2015. doi: 10.1117/1.JATIS.1.1.014003.

[5] Jon M. Jenkins, Joseph D. Twicken, Sean McCauliff, Jennifer Campbell, Dwight Sanderfer, David Lung, Masoud Mansouri-Samani, Forrest Girouard, Peter Tenenbaum, Todd Klaus, Jeffrey C. Smith, Douglas A. Caldwell, A. D. Chacon, Christopher Henze, Cory Heiges, David W. Latham, Edward Morgan, Daryl Swade, Stephen Rinehart, and Roland Vanderspek. The TESS science processing operations center. In *Software and Cyberinfrastructure for Astronomy IV*, volume 9913 of *Proceedings of the SPIE*, page 99133E, 2016. doi: 10.1117/12.2233418.

[6] Lightkurve Collaboration, José Vinícius de Miranda Cardoso, Christina Hedges, Michael Gully-Santiago, Nicholas Saunders, Ann Marie Cody, Thomas Barclay, Oliver Hall, Sheila Sagear, Emma Turtelboom, Johnny Zhang, Anastasios Tzanidakis, Kenneth Mighell, Jeff Coughlin, Keaton Bell, Zachory Berta-Thompson, Peter Williams, Jessie Dotson, and Geert Barentsen. Lightkurve: Kepler and TESS time series analysis in Python. Astrophysics Source Code Library, record ascl:1812.013, 2018. ascl:1812.013.

[7] Abraham Savitzky and Marcel J. E. Golay. Smoothing and Differentiation of Data by Simplified Least Squares Procedures. *Analytical Chemistry*, 36(8):1627–1639, 1964. doi: 10.1021/ac60214a047.

[8] G. Kovács, S. Zucker, and T. Mazeh. A box-fitting algorithm in the search for periodic transits. *Astronomy & Astrophysics*, 391:369–377, 2002. doi: 10.1051/0004-6361:20020802.

[9] Astropy Collaboration, Adrian M. Price-Whelan, Pey Lian Lim, Nicholas Earl, Nathaniel Starkman, Larry Bradley, David L. Shupe, Aarya A. Patil, Lia Corrales, C. E. Brasseur, Maximilian Nöthe, Axel Donath, Erik Tollerud, Brett M. Morris, Adam Ginsburg, Eero Vaher, Benjamin A. Weaver, James Tocknell, William Jamieson, Marten H. van Kerkwijk, Thomas P. Robitaille, Bruce Merry, Matteo Bachetti, H. Moritz Günther, and Thomas L. Aldcroft. The Astropy Project: Sustaining and Growing a Community-Oriented Open-Source Project and the Latest Major Release (v5.0) of the Core Package. *The Astrophysical Journal*, 935(2):167, 2022. doi: 10.3847/1538-4357/ac7c74.

[10] Kaisey Mandel and Eric Agol. Analytic Light Curves for Planetary Transit Searches. *The Astrophysical Journal Letters*, 580(2):L171–L175, 2002. doi: 10.1086/345520.

[11] Laura Kreidberg. batman: BAsic Transit Model cAlculatioN in Python. *Publications of the Astronomical Society of the Pacific*, 127(957):1161–1165, 2015. doi: 10.1086/683602.

[12] Pauli Virtanen, Ralf Gommers, Travis E. Oliphant, Matt Haberland, Tyler Reddy, David Cournapeau, Evgeni Burovski, Pearu Peterson, Warren Weckesser, Jonathan Bright, Stéfan J. van der Walt, Matthew Brett, Joshua Wilson, K. Jarrod Millman, Nikolay Mayorov, Andrew R. J. Nelson, Eric Jones, Robert Kern, Eric Larson, C. J. Carey, İlhan Polat, Yu Feng, Eric W. Moore, Jake VanderPlas, Denis Laxalde, Josef Perktold, Robert Cimrman, Ian Henriksen, E. A. Quintero, Charles R. Harris, Anne M. Archibald, Antônio H. Ribeiro, Fabian Pedregosa, and Paul van Mulbregt. SciPy 1.0: fundamental algorithms for scientific computing in Python. *Nature Methods*, 17:261–272, 2020. doi: 10.1038/s41592-019-0686-2.

[13] Daniel Foreman-Mackey, David W. Hogg, Dustin Lang, and Jonathan Goodman. emcee: The MCMC Hammer. *Publications of the Astronomical Society of the Pacific*, 125(925): 306–312, 2013. doi: 10.1086/670067.